Magnetic Resonance Imaging 58 (2019) 148–155

Contents lists available at ScienceDirect

Magnetic Resonance Imaging

journal homepage: www.elsevier.com/locate/mri

Original contribution

Refractory diet-dependent changes in neural microstructure: Implications for microstructural endophenotypes of neurologic and psychiatric disease

Maribel Torres-Velázquez[a], Emily A. Sawin[b], Jacqueline M. Anderson[b], John-Paul J. Yu[a,b,c,d,*]

[a] Department of Biomedical Engineering, College of Engineering, University of Wisconsin–Madison, Madison, WI 53706, USA
[b] Department of Radiology, University of Wisconsin School of Medicine and Public Health, Madison, WI 53705, USA
[c] Neuroscience Training Program, Wisconsin Institutes for Medical Research, University of Wisconsin–Madison, Madison, WI 53705, USA
[d] Department of Psychiatry, University of Wisconsin School of Medicine and Public Health, Madison, WI 53705, USA

ARTICLE INFO

Keywords:
Diet
Diffusion tensor imaging
Translational studies
Psychiatric disease

ABSTRACT

Alterations in gut microbiome populations *via* dietary manipulation have been shown to induce diet-dependent changes in white matter microstructure. The purpose of this study is to examine the durability of these diet-induced microstructural alterations. We implemented a crossover experimental design where post-weaned male rats were assigned to one of four experimental diets. Following the administration of experimental diets and again following crossover and resumption of a normal diet, brains were imaged *ex-vivo* with diffusion tensor imaging. Following standard image preprocessing, tract-based spatial statistics and region-of-interest measurements were then calculated for all diffusion tensor indices. Voxel-wise differences in FA were identified in the high fat diet group when compared to animals receiving a control diet. Following crossover, there were new voxel-wise changes in both FA and TR that do not correspond to the regions previously identified. Animals crossed over from the high fiber diet demonstrate widespread and global changes in the diffusion tensor that stand in stark contrast to the minimal changes identified before crossover. While no significant differences between any of the diffusion metrics were identified in the high protein group before crossover, statistically significant decreased RD values were observed following resumption of a normal diet. Diet-induced changes in neural microstructure are durable changes that are unrecoverable following the resumption of a normal diet. We further show that in certain experimental diets, resumption of a normal diet can lead to further marked and unanticipated changes in white matter microstructure.

1. Introduction

Diet has long been recognized as an important modulator of central nervous system (CNS) function. Reductions in brain synaptic plasticity caused by a disruption of insulin-sensitive processes has been associated with the consumption of a high fat diet [1] and a low calorie diet promotes the growth and development of nervous tissue while increasing the brain-derived neurotropic factor (BDNF) levels in adult rats [2]. A maternal high fat diet has also been associated with social behavior deficits in mice [3]. Diet has also been shown to induce changes in the composition of the gut microbiome in as little as 24 h [4] and can subsequently shape complex social and emotional behavior in both mice and humans [5,6]. Diet-induced changes in the gut microbiome are also associated with the development and exacerbation of several neurologic and psychiatric diseases including anxiety and depression [5–10] and are linked to alterations in white matter microstructure [11] and region-specific changes in neural microstructure [12].

With well-established associations between diet, diet-dependent gut microbiome populations, and neurological disease and neuropsychiatric illness, the concomitant changes in neural tissue microstructure occurring parallel to these changes in the composition of the gut microbiome have not been fully characterized. Previous work has demonstrated both diet-dependent and microbe-specific induced changes in white matter microstructure [12] but little is known about the durability of these structural changes. We sought to further examine the durability and degree of plasticity of these diet-induced microstructural alterations. Towards these ends, we implemented a crossover experimental design where post-weaned male rats were imaged with diffusion tensor imaging (DTI) following the administration of four different experimental diets and again after they were crossed over to a normal diet. We hypothesized that diet would have a minimal impact on neural microstructure, especially in the crossover group after animals resumed

* Corresponding author at: Department of Radiology, Division of Neuroradiology, University of Wisconsin School of Medicine and Public Health, 600 Highland Avenue, Madison, WI 53792-3252, USA.
E-mail address: jpyu@uwhealth.org (J.-P.J. Yu).

https://doi.org/10.1016/j.mri.2019.02.006
Received 2 December 2018; Received in revised form 23 January 2019; Accepted 14 February 2019
0730-725X/

Table 1
Composition of experimental diets. Elemental composition for the control, high fat, high fiber, and high protein diets. The control diet is a diet derived from AIN-93G, a standard widely-used rodent chow formula.

Ingredients (g/kg)	High fat diet[a] (5.3 kcal/g)	High fiber diet (2.5 kcal/g)	High protein diet (3.7 kcal/g)	Control diet (3.8 kcal/g)
Casein	200	200	793	200
L-Cystine	3	3	0	3
Corn starch	92.178	152.234	10.234	392.234
Maltodextrin	182	52	12	132
Sucrose	70	70	12	100
Soybean oil	10	70	70	70
Lard	340	0	0	0
Cellulose	50	400	50	50
Mineral mix, AIN-93G-MX (94046)	35	35	35	35
Vitamin mix, AIN-93-VX (94047)	15	15	15	15
Choline bitartrate	2.75	2.75	2.75	2.75
Vitamin K1, phylloquinone	0.002	0.002	0.002	0.002
TBHQ, antioxidant	0.07	0.014	0.014	0.014
Total (g)	1000	1000	1000	1000

[a] All custom diets from Teklad (Madison, WI, USA): TD97184, TD150669, TD150670, TD150671.

a normal diet. Unexpectedly, we found that diet-induced changes in neural microstructure to be durable changes that are unrecoverable following the resumption of a normal diet. We further show that in certain experimental diets, a return to a normal diet further exacerbates changes in white matter microstructure. The constellation of these findings demonstrates the complex role of diet in the bidirectional communication of the gut-brain axis and highlights unexpected challenges in the search for and application of microstructural endophenotypes of neurologic and neuropsychiatric disease.

2. Materials and methods

2.1. Animals and experimental design

Animals were housed and cared for in an AAALAC-accredited facility and all animal experiments were conducted in accordance with local institutional IACUC-approved protocols. Immediately following weaning, male outbred Sprague-Dawley littermate rats ($n = 44$, Charles River, Wilmington, MA, USA), were singly housed and randomized to one of four purified and irradiated diets: a control (chemically purified), high fat, high fiber, and high protein, low carbohydrate diet (Table 1). Male animals were chosen to avoid potentially confounding estrous effects; animals were singly housed to circumvent confounding effects of rat coprophagy and its impact on gut microbiome populations. Post-weaning, all animals were fed their assigned experimental diet for a total of 3-weeks with free access to water and their assigned diet [12]; animals were maintained on a 12:12-h light-dark cycle. At post-natal day (PND) 42, animals from each diet cohort ($n = 20$, $n = 5$ per diet group, PRE) were brought to a surgical plane of anesthesia and transcardially perfused with ice-cold 4% paraformaldehyde (PFA). Brains were then dissected from the cranial vault, post-fixed in 4% PFA, and stored at 4 °C. The remaining animals ($n = 24$, $n = 6$ per diet group, POST) were crossed over and placed on the control diet for an additional 21 days, whereupon the brains were dissected in a similar fashion (Fig. 1). Prior to *ex-vivo* imaging (48 h), brains were serially washed in 1× PBS to minimize the attenuating effects of fixative solution and placed in a custom-built filled with Fluorinert (FC-3283, 3 M, USA) to minimize magnetic susceptibility.

2.2. Imaging and data acquisition

Ex-vivo diffusion tensor imaging (DTI) acquisition was performed on 2–3 brains simultaneously using a 4.7-T Agilent MRI system and 3.5-cm diameter quadrature volume RF coil. All imaging data was obtained concurrently on the same MR system. A multi-slice spin echo sequence was employed to obtain the diffusion-weighted imaging (DWI) data. MRI acquisition parameters include: repetition time: 2000 ms; echo time: 24.17 ms; field of view: 32 mm × 32 mm; image dimension: 128 × 128 × 100; and resolution: 0.25 mm (isotropic). Diffusion was encoded along 30 non-collinear directions ($b = 1200\ s{\cdot}mm^{-2}$) and three additional non-diffusion weighted measurements ($b = 0\ s{\cdot}mm^{-2}$). The acquisition was averaged across two repeats for a total scanning time of approximately 11 h.

2.3. Image preprocessing and spatial normalization

Following image data acquisition, individual diffusion weighted (DWI) images were co-registered and corrected for eddy currents distortions using the affine registration tool [13] from the FMRIB software library (FSL; http://fsl.fmrib.ox.ac.uk/fsl/fslwiki). Additional preprocessing was performed to correct for rotations in gradient directions [14]. Following corrections, the diffusion tensor was fitted using FSL and DTI output volumes were converted to NIfTI tensor format. The NIfTI tensor format is compatible with the DTI-TK software platform (http://dti-tk.sourceforge.net/pmwiki/pmwiki.php) which was then implemented for the normalization and registration of the data sets. The normalization and registration of the data was performed separately for the PRE and POST crossover groups. Diffusivity units were confirmed to be within $10^{-3}\ mm^2/s$ as required by the DTI-TK normalization routine. A study specific tensor template was estimated from all individual data sets from each sample within the control group. The template was then used to normalize and register each individual DTI tensor volume using the DTI-TK tensor-based registration routine. The DTI-TK registration routine is a non-parametric, diffeomorphic deformable image registration [15], with enhanced performance over other registration tools [16].

2.4. Tract-based spatial statistics (TBSS)

Voxel-wise statistical analysis of both the PRE and POST crossover data were carried out using TBSS as recommended by Bach et al. [17]. A TBSS pipeline was implemented replacing the traditional registration tool (FSL's FNIRT) by the DTI-TK registration routine, which improves alignment quality. The rest of the pipeline was implemented using the standard parameters in FSL, including a 0.2 FA threshold to create the white matter skeleton [18]. A permutation test ($n = 252$) corrected for multiple comparisons and threshold-free cluster enhancement (TFCE) [19] was employed with FSL's Randomize for inter-group comparison ($\alpha < 0.05$ for significance).

2.5. Region of interest analysis

The UNC Rat Atlas [20] was utilized to extract DTI measures from regions-of-interest (ROIs) in the brain. Before automated volumetric segmentation of the brain, the atlas was normalized to subject common space and ROIs masked. Mean values of diffusivity were then computed for each individual subject in 6 predetermined regions of the brain (hippocampus, external capsule, internal capsule, thalamus, neocortex, and corpus callosum). These values were calculated for each hemisphere of the brain for a total of 12 ROIs. A two-tailed, two-sample, and unequal variance Student's *t*-test was performed comparing FA (fractional anisotropy), AD (axial diffusivity), RD (radial diffusivity), and TR (trace; mean diffusivity [MD] × 3) mean values in each diet group against age-sex-matched controls for both the PRE and POST diet experimental groups. Raw p-values were reported and adjusted p-values

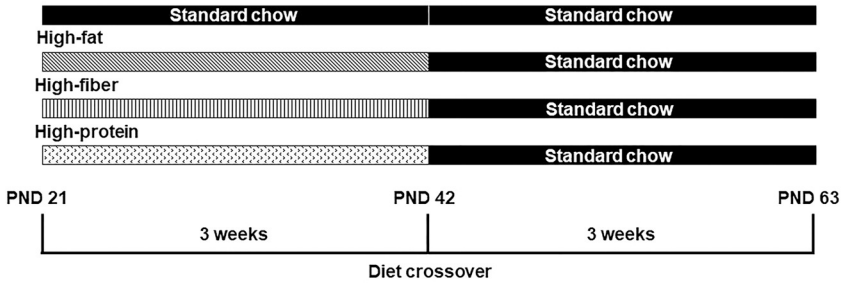

Fig. 1. Experimental design. Male rats were fed the experimental diets immediately post-weaning for a total of 21 days. At post natal day (PND) 42, animals from each diet cohort (total n = 20, n = 5 per diet group, PRE) were sacrificed and brains dissected. The remaining animals (total n = 24, n = 6 per diet group, POST) were crossed over and remained on the control diet for an additional 21 days, whereupon the brains were isolated in a similar fashion. Voxel-wise TBBS analysis was performed between animals on the control/standard chow diet and those on either a high fat, high fiber, or high protein diet at PND 24 (PRE diet group) and PND 63 (POST diet group).

(correcting for multiple comparisons) were calculated using a Benjamini-Hochberg false discovery rate (FDR) correction (FDR = 0.05).

3. Results

3.1. Refractory diet-dependent changes in white matter structural integrity

To uncover diet-induced changes in neural tissue microstructure, *ex-vivo* whole brain DTI was performed followed by voxel-wise and ROI analyses on samples from both the PRE and POST diet crossover groups (Fig. 1). In a crossover experimental design, animals from the PRE diet group were compared against animals from the control diet group at PND 42 following 3-weeks of experimental diet administration. To next examine the durability of diet-induced changes in neural microstructure, all animals on experimental diets were crossed over to a control diet for an additional 3-weeks (POST diet group) and subsequently compared to age- and sex-matched control animals that were exclusively fed a control diet.

Statistically significant voxel-wise differences in fractional anisotropy (FA) were identified in the high fat diet group when compared to animals receiving a control diet (Fig. 2a). Following 3-weeks of a high fat diet, there is evidence of decreased FA through a small portion of the right neocortex accompanied by decreased RD (radial diffusivity) (Fig. S1b). When animals on a high fat diet are crossed over to the control diet, interestingly, there are new voxel-wise changes in both FA and TR (trace; mean diffusivity [MD] × 3) that do not correspond to the areas of previous FA change see in the PRE diet cohort (Fig. 2c–d); suggesting that the microstructural changes appreciated as a consequence of a high fat diet are durable and refractory to diet normalization. These voxel-wise changes seen in the crossover group correspond to statistically significant higher FA in the right superior neocortex, right internal capsule, right hippocampus, left inferior neocortex, left hypothalamus, and brainstem with increased TR in the corpus callosum, right and left external capsule, and left fimbria. As expected, increased FA and TR values in the POST high fat group are coupled with an increase in AD values (Fig. S1e).

Animals randomized to the high fiber diet group demonstrate decreased TR values through the right neocortex and external capsule (Fig. 3b) with decreases in RD also in the right neocortex and external capsule with extension into the left hemisphere (Fig. S2b) following 3-weeks on a high fiber diet. No significant differences in FA were identified. Surprisingly, animals crossed over from the high fiber diet demonstrated widespread and global changes in the diffusion tensor with decreased FA, TR, AD and RD, and increased RD that stand in stark contrast to the minimal changes see in the high fiber PRE group. These FA changes encompass the neocortex, external capsule, corpus callosum, and rest of the forebrain (Fig. 3c). Decreased TR values are observed at the central gray and brainstem (Fig. 3d). By and large, areas of decreased FA and TR in the high fiber POST group are accompanied with concomitant changes in AD and RD (Fig. S2e–f). While no significant differences between any of the DTI metrics were identified in the PRE high protein group, statistically significant decreased RD values were observed throughout the brainstem after crossover (Fig. S3).

3.2. Diet contributes to significant changes in specific regions of interest in the brain

Voxel-wise TBSS analysis uncovered global differences in the diffusion tensor between experimental and age- and sex-matched control groups in both the PRE and POST diet crossover groups. To further explore the contribution of diet to neural microstructure, a ROI analysis was next performed to explicitly examine how changes in diet impact neural microstructure in regions of the brain implicated in both neurologic and neuropsychiatric illness. A total of six regions of the brain were *a priori* selected to further analysis: the hippocampus, external capsule, internal capsule, thalamus, neocortex, and corpus callosum. Mean values of FA, AD, RD, and TR were computed for each individual subject in each priori selected region. The mean diffusivity values were calculated for each hemisphere of the brain for a total of 12 ROIs. Within the high fat diet group, an increase in FA in the left thalamus is observed in the PRE high fat diet when compared to the corresponding control group (Table 2). In addition, decreased FA is observed in the right hippocampus and right neocortex, following crossover to the control diet, along with increased FA in the left internal capsule (Table 3). While no significant TR differences were observed PRE crossover, the POST crossover high fat group shows an increase in TR at the right external capsule. Accounting for multiple comparisons (Benjamini-Hochberg correction with FDR = 0.05), statistically significant decreased FA in the left thalamus and right neocortex, PRE and POST crossover respectively, were sustained. Although a significant increase in FA at the right neocortex ROI appears to be contradictory to the TBSS results, we could expect this segmentation-based test to be more specific and revealing important neuroanatomical alterations. Additional significant AD and RD values were obtained prior to FDR correction for the high fat group, PRE (Table S1) and POST crossover (Table S2).

Within the high fiber diet cohorts, a significant decrease in FA is seen in the right thalamus, left thalamus, and left neocortex along with increased TR at the right internal capsule (Table 1). Following diet crossover, the high fiber group demonstrated widespread significant decreases in FA in the right corpus callosum and left external capsule and increased FA in the left neocortex (Table 2). An increase in TR is also observed in the right hippocampus, right thalamus, and left external capsule, following the diet crossover. After controlling for multiple comparisons, only the decreased FA in the left thalamus in the PRE high fiber group remains significant. Other AD and RD ROIs within the high fiber group demonstrated statistical significance with increased RD in the right hippocampus and left external capsule following diet crossover and FDR correction (Table S2). The high protein group shows a significant decrease in FA at the left internal capsule and left thalamus before crossover (Table 1) and a decrease in FA at the left external capsule after crossover (Table 2). No significant TR values were observed, PRE or POST crossover; and only a significant increase in RD at the left internal capsule is detected for the PRE high protein group after FDR correction (Table S1).

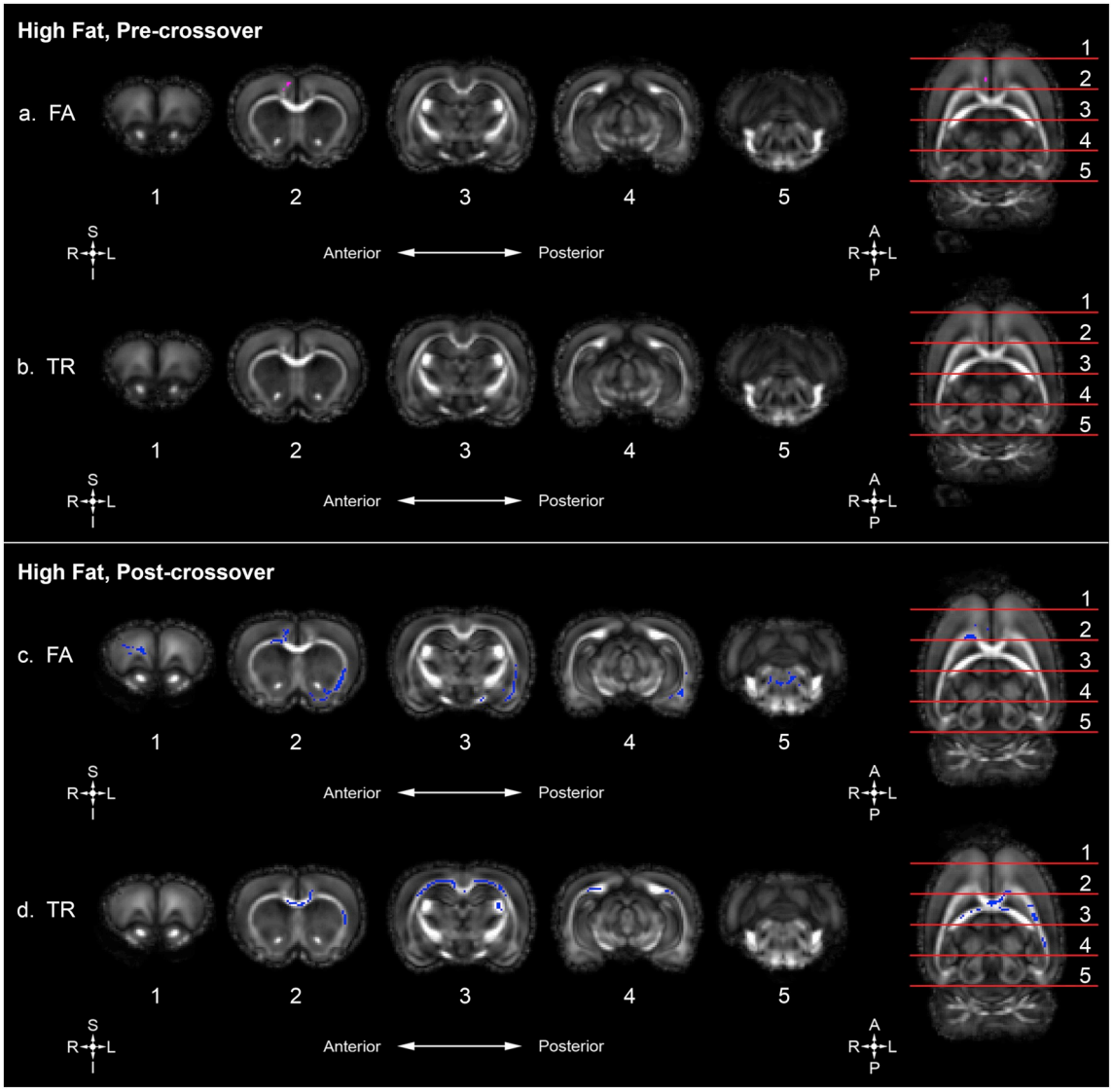

Fig. 2. High fat diet induces refractory changes in white matter microstructural integrity. Whole-brain voxel-wise tract-based spatial statistics (TBBS) analysis was performed between animals on the control/standard chow diet and those on a high fat diet at PND 24 (PRE diet group) and PND 63 (POST diet group). Statistically significant differences in fractional anisotropy (FA) and trace (TR; trace: mean diffusivity [MD] × 3) were calculated for the (**a–b**) PRE high fat and (**c–d**) POST high fat diet groups (family-wise error corrected, $\alpha < 0.05$). Voxels of increased (blue) and decreased (magenta) FA or TR as compared to controls are shown. (For interpretation of the references to color in this figure legend, the reader is referred to the web version of this article.)

4. Discussion

The role of diet in the bidirectional communication between the gastrointestinal microbial environment and the central nervous system involves complex neuronal, endocrine, and immunological processes. Notably, the interactions between diet, subsequent changes in the composition of the gut microbiome, and the CNS is consequential, one capable of modulating system-level behavior in animals [21] and also one that is able to induce microstructural changes in the brain [11,12]. To build upon these findings, we next explored the durability of these microstructural changes in the brain so as to determine whether subsequent changes in diet – specifically resuming a normal diet – would be sufficient to rescue our previously observed changes in neural microstructure. To this end, we implemented a crossover experimental design to examine the durability of diet-induced microstructural changes to the brain. We anticipated that diet-induced changes would be observed (both in our TBSS and ROI analysis), with decreased FA suggesting a decrease in microstructural integrity as a consequence of each experimental diet but that these changes would be temporary and recoverably following a return to a normal diet. To our surprise, we found that many of the diet-induced microstructural changes are durable and are unable to be rescued with a return to a normal balanced diet (in the crossover arm). In some cases, we also saw an unexpected marked *increase* in microstructural change following the resumption of a normal diet that demonstrates an extraordinary mixture of both plastic and durable microstructural changes that can be attributable to changes in diet.

Changes in diet and subsequent downstream changes in the gut microbiome may contribute to alterations in neural microstructure due to the production of secondary metabolites generated by diet-dependent shifts in the composition of the gut microbiome. These metabolites, including short chain fatty acids (SCFAs), which are produced by the bacterial fermentation of dietary carbohydrates that are also seen in in high fiber diets [22–24], are potent molecules known to alter neuronal excitability [25]. Of particular interest is butyrate, a SCFA produced by fermentation of non-digestible fiber by bacteria in the colon that also functions as a histone deacetylase (HDAC) inhibitor, an energy metabolite to produce ATP, and a G protein-coupled receptor (GCPR)

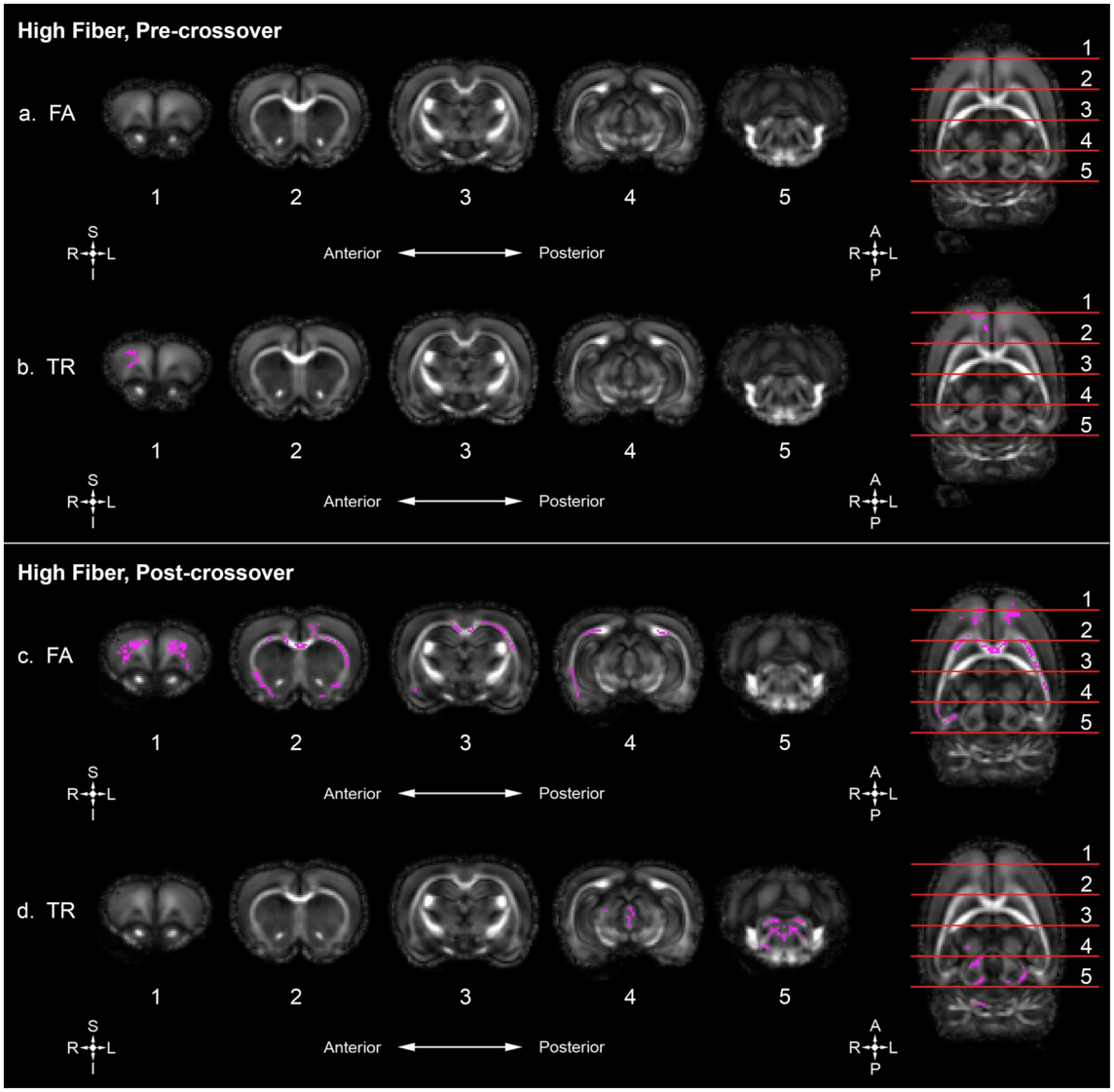

Fig. 3. High fiber diet induces refractory changes in white matter microstructural integrity. Whole-brain voxel-wise tract-based spatial statistics (TBBS) analysis was performed between animals on the control/standard chow diet and those on a high fiber diet at PND 24 (PRE diet group) and PND 63 (POST diet group). Statistically significant differences in fractional anisotropy (FA) and trace (TR; trace: mean diffusivity [MD] × 3) were calculated for the (**a**–**b**) PRE high fiber and (**c**–**d**) POST high fiber diet groups (family-wise error corrected, $\alpha < 0.05$). Voxels of decreased FA or TR (magenta) as compared to controls are shown. (For interpretation of the references to color in this figure legend, the reader is referred to the web version of this article.)

activator [26] and has also been shown to decrease blood brain barrier (BBB) permeability in germ free mice while simultaneously increasing brain histone acetylation and expression of tight junctions proteins, such as occludin and claudin 5 [27]. As many of our most pronounced changes were seen in animals returning to a normal diet following 3-weeks of a high fiber diet, a potential hypothesis to explain these changes would be the dramatic decrease in circulating butyrate and concomitant increased porosity in the BBB, which would allow for a greater influx of other factors that could then secondarily bring about the observed changes in neural tissue microstructure. Future studies exploring how changes in the composition of the gut microbiome and how the relative abundance of different bacterial species can alter the underlying porosity of the BBB would begin to answer questions regarding the mechanism whereby changes in the gut microbiome can induce changes within the brain.

Gastrointestinal and psychiatric illnesses such as anxiety disorders, major depressive disorder, bipolar disorder, autism spectrum disorder, and schizophrenia share a surprising degree of comorbidity that suggests a causal association between microbiome populations and the development of psychopathologies [28–31]. Complementary to the voxel-wise diet-dependent microstructural changes observed, our subsequent ROI analyses revealed specific neuroanatomical alterations in the brain that may be linked to neurologic and psychiatric diseases. A high fat diet has been previously associated with deficits in hippocampus-dependent memory/learning and mood states [32–35]. Our findings buttress these reports by uncovering a significant decrease in FA at the right hippocampus for the high fat group following diet crossover. Likewise, high fiber diets are known to have beneficial effects on memory and cognition [26] with previous work demonstrating children exposed to a high fiber diet exhibited better cognitive control than children on a low fiber diet [36]. Surprisingly, our ROI analysis highlights the thalamus, a contributor of cognitive processes, such as attention, speed of information, and memory [37], as a region with statistically significant decreased FA in animals fed a high fiber diet for 3 weeks. These results suggest that interventions based singularly on diet may not represent a viable treatment option for some neurologic and psychiatric diseases despite promising evidence in certain cognitive and behavioral processes.

Table 2
Regions-of-interest (ROIs) analysis for PRE diet crossover groups. All values are mean ± s.e.m. Units of measure for TR are [10^{-3} mm^2/s]. Bolded and italicized p-values are statistically significant. Starred p-values are statistically significant after controlling the false discovery rate with the Benjamini-Hochberg procedure (false discovery rate = 0.05). Regions of interest (ROIs) correspond to ROIs derived from the P72 UNC Atlas. Diffusion measure abbreviations: Hemi. = hemisphere; FA = fractional anisotropy; TR = trace (mean diffusivity [MD] × 3). ROI abbreviations: HC = Hippocampus; EC = External Capsule; IC = Internal Capsule; T = Thalamus; NC = Neocortex; CC = Corpus Callosum. For all sample groups, n = 5.

DTI measure	Hemi.	ROI	Mean (± SEM)				p-Value		
			Control	High fat	High fiber	High protein	High fat	High fiber	High protein
FA	Right	HC	0.30571 (± 0.00102)	0.30951 (± 0.0036)	0.30509 (± 0.00146)	0.30845 (± 0.00211)	0.36099	0.73472	0.28941
		EC	0.45738 (± 0.00243)	0.45753 (± 0.00057)	0.45531 (± 0.00414)	0.45406 (± 0.00098)	0.95439	0.68035	0.25867
		IC	0.44523 (± 0.00244)	0.44335 (± 0.00229)	0.44614 (± 0.00114)	0.44767 (± 0.00195)	0.59016	0.74722	0.45823
		T	0.37672 (± 0.00104)	0.37413 (± 0.00196)	0.37214 (± 0.00111)	0.37526 (± 0.0009)	0.28608	***0.01657***	0.31893
		NC	0.29114 (± 0.00167)	0.28834 (± 0.00054)	0.29341 (± 0.00083)	0.28972 (± 0.00085)	0.17309	0.27092	0.47825
		CC	0.52253 (± 0.00059)	0.52156 (± 0.00271)	0.52056 (± 0.00145)	0.52192 (± 0.00158)	0.74327	0.26211	0.73532
	Left	HC	0.32909 (± 0.0004)	0.32818 (± 0.00051)	0.32849 (± 0.00057)	0.32845 (± 0.00106)	0.20216	0.41544	0.59584
		EC	0.41067 (± 0.00445)	0.41852 (± 0.00518)	0.41867 (± 0.00221)	0.41238 (± 0.00355)	0.28455	0.16015	0.77157
		IC	0.56526 (± 0.00194)	0.56864 (± 0.00581)	0.56382 (± 0.00469)	0.55423 (± 0.003)	0.60526	0.78715	***0.01805***
		T	0.35199 (± 0.00122)	0.34497 (± 0.00083)	0.34426 (± 0.00051)	0.34707 (± 0.00045)	***0.00208****	***0.00168****	***0.0128***
		NC	0.28975 (± 0.00141)	0.29034 (± 0.00228)	0.28544 (± 0.00103)	0.28889 (± 0.00142)	0.83204	***0.04119***	0.67933
		CC	0.56878 (± 0.00221)	0.57108 (± 0.00142)	0.57014 (± 0.0017)	0.57066 (± 0.00137)	0.41102	0.63939	0.49349
TR	Right	HC	0.36516 (± 0.00054)	0.3668 (± 0.00077)	0.36453 (± 0.00065)	0.36661 (± 0.00071)	0.12037	0.47959	0.14353
		EC	0.28571 (± 0.00068)	0.28629 (± 0.00067)	0.28785 (± 0.00098)	0.28595 (± 0.00061)	0.56099	0.11343	0.79917
		IC	0.29937 (± 0.0006)	0.29974 (± 0.00065)	0.30131 (± 0.00041)	0.30114 (± 0.0006)	0.6838	***0.0313***	0.06973
		T	0.35771 (± 0.00029)	0.35787 (± 0.00074)	0.35764 (± 0.00058)	0.3585 (± 0.00068)	0.84801	0.92472	0.32717
		NC	0.32101 (± 0.00071)	0.32086 (± 0.00035)	0.32221 (± 0.00094)	0.31918 (± 0.00068)	0.8608	0.34305	0.10145
		CC	0.27201 (± 0.00044)	0.27177 (± 0.00071)	0.27285 (± 0.00077)	0.27189 (± 0.00081)	0.78014	0.37682	0.90151
	Left	HC	0.37408 (± 0.00075)	0.37489 (± 0.00115)	0.37469 (± 0.00078)	0.37324 (± 0.00085)	0.57565	0.58835	0.47937
		EC	0.29986 (± 0.00077)	0.29862 (± 0.00083)	0.30012 (± 0.00069)	0.29885 (± 0.00077)	0.30586	0.805	0.37965
		IC	0.29258 (± 0.00051)	0.29246 (± 0.0007)	0.29401 (± 0.0005)	0.29396 (± 0.00029)	0.89902	0.0795	0.05329
		T	0.36053 (± 0.00056)	0.36046 (± 0.00073)	0.36114 (± 0.00074)	0.36079 (± 0.00072)	0.94917	0.52648	0.78088
		NC	0.32448 (± 0.00095)	0.32443 (± 0.00051)	0.32611 (± 0.00037)	0.32491 (± 0.00116)	0.96196	0.16605	0.78014
		CC	0.26192 (± 0.00071)	0.26083 (± 0.00067)	0.26062 (± 0.00069)	0.26099 (± 0.00052)	0.30119	0.22861	0.32528

The work described herein is also bears important experimental considerations for the neuroscience and neuroimaging community. Quantitative microstructural neuroimaging techniques such as diffusion tensor imaging are often utilized to detect imaging endophenotypes across a broad range of neurologic and psychiatric diseases and the sensitivity of diffusion tensor imaging, coupled with its bias-free automated analysis, makes this an established and widespread clinical and experimental technique. Diffusion tensor techniques also serve as the

Table 3
Regions-of-interest (ROIs) analysis for POST diet crossover groups. All values are mean ± s.e.m. Units of measure for TR are [10^{-3} mm^2/s]. Bolded and italicized p-values are statistically significant. Starred p-values are statistically significant after controlling the false discovery rate with the Benjamini-Hochberg procedure (false discovery rate = 0.05). Regions of interest (ROIs) correspond to ROIs derived from the P72 UNC Atlas. Diffusion measure abbreviations: Hemi. = hemisphere; FA = fractional anisotropy; TR = trace (mean diffusivity [MD] × 3). ROI abbreviations: HC = Hippocampus; EC = External Capsule; IC = Internal Capsule; T = Thalamus; NC = Neocortex; CC = Corpus Callosum. For all sample groups, n = 6.

DTI measure	Hemi.	ROI	Mean (± SEM)				p-Value		
			Control	High fat	High fiber	High protein	High fat	High fiber	High protein
FA	Right	HC	0.30734 (± 0.00121)	0.30386 (± 0.00074)	0.30771 (± 0.00072)	0.30726 (± 0.00105)	***0.0382***	0.80275	0.95717
		EC	0.45699 (± 0.0008)	0.45788 (± 0.00061)	0.45729 (± 0.00172)	0.45898 (± 0.00112)	0.40148	0.88192	0.18226
		IC	0.44601 (± 0.0035)	0.44888 (± 0.0015)	0.45195 (± 0.00208)	0.44865 (± 0.00182)	0.4764	0.18239	0.52457
		T	0.37145 (± 0.00087)	0.36995 (± 0.00048)	0.37414 (± 0.00177)	0.37295 (± 0.00202)	0.16836	0.21403	0.51719
		NC	0.28903 (± 0.00062)	0.28542 (± 0.00043)	0.28772 (± 0.00146)	0.28805 (± 0.00103)	***0.001****	0.43446	0.43782
		CC	0.52227 (± 0.00069)	0.52303 (± 0.0013)	0.51947 (± 0.0007)	0.52168 (± 0.00092)	0.62077	***0.0176***	0.62318
	Left	HC	0.32857 (± 0.00062)	0.32853 (± 0.00059)	0.32832 (± 0.00073)	0.32812 (± 0.00046)	0.96599	0.79671	0.56802
		EC	0.42132 (± 0.00082)	0.41555 (± 0.00378)	0.40644 (± 0.00343)	0.40902 (± 0.00438)	0.19098	***0.00656***	***0.03696***
		IC	0.56353 (± 0.00476)	0.57836 (± 0.00383)	0.55882 (± 0.0044)	0.57433 (± 0.00465)	***0.03662***	0.48402	0.13565
		T	0.34697 (± 0.00095)	0.3479 (± 0.00062)	0.3466 (± 0.00113)	0.34694 (± 0.0006)	0.43053	0.81063	0.98378
		NC	0.28669 (± 0.00063)	0.28771 (± 0.0009)	0.29087 (± 0.0013)	0.29028 (± 0.00171)	0.37671	***0.0229***	0.0945
		CC	0.5732 (± 0.00176)	0.5704 (± 0.00131)	0.56935 (± 0.00185)	0.56882 (± 0.00116)	0.23242	0.16202	0.06879
TR	Right	HC	0.36527 (± 0.00089)	0.36484 (± 0.00064)	0.36823 (± 0.00046)	0.36585 (± 0.00092)	0.70427	***0.01995***	0.66239
		EC	0.28632 (± 0.00026)	0.28741 (± 0.00023)	0.28683 (± 0.00023)	0.28634 (± 0.00022)	***0.01146***	0.17152	0.95896
		IC	0.30134 (± 0.00049)	0.30151 (± 0.00022)	0.30017 (± 0.0003)	0.30083 (± 0.00056)	0.76399	0.07503	0.5113
		T	0.35663 (± 0.0005)	0.35675 (± 0.00022)	0.3583 (± 0.00035)	0.35746 (± 0.00052)	0.82363	***0.02298***	0.27671
		NC	0.32094 (± 0.00051)	0.3204 (± 0.00026)	0.32167 (± 0.00059)	0.32142 (± 0.0004)	0.37644	0.37343	0.48129
		CC	0.27229 (± 0.00043)	0.27213 (± 0.00036)	0.27199 (± 0.00052)	0.27216 (± 0.00063)	0.7813	0.67055	0.8699
	Left	HC	0.37382 (± 0.0006)	0.37329 (± 0.00067)	0.37394 (± 0.0006)	0.37433 (± 0.00075)	0.56942	0.8874	0.60926
		EC	0.29895 (± 0.00061)	0.29987 (± 0.00079)	0.30183 (± 0.00077)	0.30116 (± 0.0008)	0.38013	***0.01571***	0.05426
		IC	0.29348 (± 0.00073)	0.29333 (± 0.00043)	0.2936 (± 0.00031)	0.29218 (± 0.00033)	0.86005	0.88123	0.14683
		T	0.36001 (± 0.00053)	0.35931 (± 0.00022)	0.3612 (± 0.0003)	0.36052 (± 0.00045)	0.26204	0.08607	0.47802
		NC	0.32509 (± 0.00059)	0.32375 (± 0.00049)	0.32534 (± 0.00086)	0.32604 (± 0.00057)	0.10887	0.82113	0.2773
		CC	0.26097 (± 0.00078)	0.2618 (± 0.0003)	0.2615 (± 0.00059)	0.26131 (± 0.00037)	0.35693	0.59891	0.70486

basis for several large ongoing neuroimaging trials including the Alzheimer's Disease Neuroimaging Initiative, the Human Connectome Project, and ENIGMA-DTI. In the work presented herein, our findings that unaccounted experimental variables such as diet are able to exert an unexpected impact on sensitive measures of diffusion tensor is an unanticipated and surprising challenge and one that bears significant consideration as we begin to interpret these neuroimaging measurements.

Although we have demonstrated that diet and subsequent changes in diet are able to exert a broad range of plastic and durable microstructural changes throughout the brain, additional analyses are needed to ascertain whether these microstructural changes can be correlated with specific gut bacterial populations [12] or if they are a result of other metabolic processes that may arise secondary to changes in diet. In particular, the caloric density (and observed accelerated weight gain) of animals on the high fat diet may have contributed to other diet-induced metabolic changes that could conceivably influence the microstructural changes seen in the high fat diet; conversely, the relative energy depleted food made available to animals in the high fiber diet could also yield a similar (opposite) effect. Despite this limitation, that we observe such significant changes in neural microstructure due to simple changes in diet remains a surprising finding and an important consideration as we begin to examine and interpret large-scale neuroimaging studies. A potential criticism of our study is the timeframe selected for diet intervention as the brain undergoes significant neurodevelopmental changes during this time (PND 21–63) thus making it difficult to disambiguate normal neurodevelopmental changes from pathologic changes arising from changes in diet. The experimental timeframe was selected, however, to address emerging evidence of the role of diet in the development of psychiatric illness, especially during childhood and early adolescence, which corresponds to the ages of the animals used in this study [5–10]. As only age-matched comparisons are made and if changes in diet have no impact on quantitative measures of neural microstructure, we would accordingly expect no differences between our age-matched groups, irrespective of diet. Our results, however, suggest otherwise and show how changes in diet can alter neurodevelopmental trajectories during a sensitive neurodevelopmental window.

5. Conclusions

Implementing a crossover experimental design, we uncovered refractory and global diet-induced changes to white matter microstructural integrity in male rats subjected to one of three experimental diets: a high fat diet, high fiber diet, and high protein diet. These data reinforce the linkage of diet with neurologic and psychopathological outcomes and diet as an important factor in the development and treatment of neurological and neuropsychiatric disorders. As we begin to examine large-scale cross-sectional and longitudinal neuroimaging data, understanding how experimental variables such as diet and the ability of diet to exert an unexpected impact on sensitive measures of diffusion tensor will be critical and important as we start to unpack and translate these neuroimaging data to the clinic and hope to reliably and faithfully interpret these neuroimaging data.

Acknowledgements

J-P.J.Y was supported by Department of Radiology at the University of Wisconsin School of Medicine and Public Health and the Brain and Behavior Research Foundation (NARSAD) Young Investigator Grant. Additional support was provided by the Clinical and Translational Science Award (CTSA) program, through the NIH National Center for Advancing Translational Sciences (NCATS), grant UL1TR002373. M.T-V. was supported under NIH awards UL1TR000427 and TL1TR000429. Additional imaging support was provided by the University of Wisconsin Carbone Cancer Center Support Grant P30CA014520. The content is solely the responsibility of the authors and does not necessarily represent the official views of the NIH.

Appendix A. Supplementary data

Supplementary data to this article can be found online at https://doi.org/10.1016/j.mri.2019.02.006.

References

[1] Liu Z, Patil IY, Jiang T, Sancheti H, Walsh JP, Stiles BL, et al. High-fat diet induces hepatic insulin resistance and impairment of synaptic plasticity. PLoS One 2015;10:e0128274.
[2] Kaptan Z, Akgün-Dar K, Kapucu A, Dedeakayoŋullari H, Batu Ş, Üzüm G. Long term consequences on spatial learning-memory of low-calorie diet during adolescence in female rats; hippocampal and prefrontal cortex BDNF level, expression of NeuN and cell proliferation in dentate gyrus. Brain Res 2015;1618:194–204.
[3] Buffington SA, Di Prisco GV, Auchtung TA, Ajami NJ, Petrosino JF, Costa-Mattioli M. Microbial reconstitution reverses maternal diet-induced social and synaptic deficits in offspring. Cell 2016;165:1762–75.
[4] David LA, Maurice CF, Carmody RN, Gootenberg DB, Button JE, Wolfe BE, et al. Diet rapidly and reproducibly alters the human gut microbiome. Nature 2014;505:559–63.
[5] Hsiao EY, McBride SW, Hsien S, Sharon G, Hyde ER, McCue T, et al. Microbiota modulate behavioral and physiological abnormalities associated with neurodevelopmental disorders. Cell 2013;155:1451–63.
[6] Tillisch K, Labus J, Kilpatrick L, Jiang Z, Stains J, Ebrat B, et al. Consumption of fermented milk product with probiotic modulates brain activity. Gastroenterology 2013;144.
[7] Whitehead WE, Palsson O, Jones KR. Systematic review of the comorbidity of irritable bowel syndrome with other disorders: what are the causes and implications? Gastroenterology 2002;122:1140–56.
[8] Collins SM, Surette M, Bercik P. The interplay between the intestinal microbiota and the brain. Nat Rev Microbiol 2012;10:735–42.
[9] Sampson TR, Mazmanian SK. Control of brain development, function, and behavior by the microbiome. Cell Host Microbe 2015;17:565–76.
[10] Gevers D, Kugathasan S, Denson LA, Vázquez-Baeza Y, Van Treuren W, Ren B, et al. The treatment-naive microbiome in new-onset Crohn's disease. Cell Host Microbe 2014;15:382–92.
[11] Fernandez-Real JM, Serino M, Blasco G, Puig J, Daunis-I-Estadella J, Ricart W, et al. Gut microbiota interacts with brain microstructure and function. J Clin Endocrinol Metab 2015;100:4505–13.
[12] Ong IM, Gonzalez JG, McIlwain SJ, Sawin EA, Schoen AJ, Adluru N, et al. Gut microbiome populations are associated with structure-specific changes in white matter architecture. Transl Psychiatry 2018;8.
[13] Jenkinson M, Bannister P, Brady M, Smith S. Improved optimization for the robust and accurate linear registration and motion correction of brain images. Neuroimage 2002;17:825–41.
[14] Leemans A, Jones DK. The B-matrix must be rotated when correcting for subject motion in DTI data. Magn Reson Med 2009;61:1336–49.
[15] Zhang Hui, Avants BB, Yushkevich PA, Woo JH, Wang Sumei, McCluskey LF, et al. High-dimensional spatial normalization of diffusion tensor images improves the detection of white matter differences: an example study using amyotrophic lateral sclerosis. IEEE Trans Med Imaging 2007;26:1585–97.
[16] Wang Y, Gupta A, Liu Z, Zhang H, Escolar ML, Gilmore JH, et al. DTI registration in atlas based fiber analysis of infantile Krabbe disease. Neuroimage 2011;55:1577–86.
[17] Bach M, Laun FB, Leemans A, Tax CMW, Biessels GJ, Stieltjes B, et al. Methodological considerations on tract-based spatial statistics (TBSS). Neuroimage 2014;100:358–69.
[18] Smith SM, Jenkinson M, Johansen-Berg H, Rueckert D, Nichols TE, Mackay CE, et al. Tract-based spatial statistics: voxel wise analysis of multi-subject diffusion data. Neuroimage 2006;31:1487–505.
[19] Smith SM, Nichols TE. Threshold-free cluster enhancement: addressing problems of smoothing, threshold dependence and localisation in cluster inference. Neuroimage 2009;44:83–98.
[20] Rumple A, Mcmurray M, Johns J, Lauder J, Makam P, Radcliffe M, et al. 3-Dimensional diffusion tensor imaging (DTI) atlas of the rat brain. PLoS One 2013;8:e67334.
[21] Hsiao EY, McBride SW, Hsien S, Sharon G, Hyde ER, McCue T, et al. Microbiota modulate behavioral and physiological abnormalities associated with neurodevelopmental disorders. Cell 2013;155:1451–63.
[22] Wolever TM, Chiasson JL. Acarbose raises serum butyrate in human subjects with impaired glucose tolerance. Br J Nutr 2000;84:57–61.
[23] Priebe MG, Wang H, Weening D, Schepers M, Preston T, Vonk RJ. Factors related to colonic fermentation of nondigestible carbohydrates of a previous evening meal increase tissue glucose uptake and moderate glucose-associated inflammation. Am J Clin Nutr 2010;91:90–7.
[24] Robertson MD, Bickerton AS, Dennis AL, Vidal H, Frayn KN. Insulin-sensitizing effects of dietary resistant starch and effects on skeletal muscle and adipose tissue metabolism. Am J Clin Nutr 2005;82:559–67.
[25] Nøhr MK, Egerod KL, Christiansen SH, Gille A, Offermanns S, Schwartz TW, et al. Expression of the short chain fatty acid receptor GPR41/FFAR3 in autonomic and

somatic sensory ganglia. Neuroscience 2015;290:126–37.
[26] Bourassa MW, Alim I, Bultman SJ, Ratan RR. Butyrate, neuroepigenetics and the gut microbiome: can a high fiber diet improve brain health? Neurosci Lett 2016;625:56–63.
[27] Braniste V, Al-Asmakh M, Kowal C, Anuar F, Abbaspour A, Toth M, et al. The gut microbiota influences blood-brain barrier permeability in mice. Sci Transl Med 2014;6:263ra158.
[28] Neufeld K-A, Foster JA. Effects of gut microbiota on the brain: implications for psychiatry. 2009;34.
[29] Kennedy PJ, Cryan JF, Dinan TG, Clarke G. Irritable bowel syndrome: a microbiome-gut-brain axis disorder? World J Gastroenterol 2014;20:14105–25.
[30] Fadgyas-Stanculete M, Buga A-M, Popa-Wagner A, Dumitrascu DL. The relationship between irritable bowel syndrome and psychiatric disorders: from molecular changes to clinical manifestations. 2014.
[31] Rogers GB, Keating DJ, Young RL, Wong M-L, Licinio J, Wesselingh S. From gut dysbiosis to altered brain function and mental illness: mechanisms and pathways. Mol Psychiatry 2016;21:1–11.
[32] Wu H, Liu Q, Kalavagunta PK, Huang Q, Lv W, An X, et al. Normal diet vs high fat diet - a comparative study: behavioral and neuroimmunological changes in adolescent male mice. Metab Brain Dis 2018;33:177–90.
[33] Kaczmarczyk MM, Machaj AS, Chiu GS, Lawson MA, Gainey SJ, York JM, et al. Methylphenidate prevents high-fat diet (HFD)-induced learning/memory impairment in juvenile mice. 2013.
[34] Boitard C, Cavaroc A, Sauvant J, Aubert A, Castanon N, Layé S, et al. Impairment of hippocampal-dependent memory induced by juvenile high-fat diet intake is associated with enhanced hippocampal inflammation in rats. 2014.
[35] Boitard C, Etchamendy N, Sauvant J, Aubert A, Tronel S, Marighetto A, et al. Juvenile, but not adult exposure to high-fat diet impairs relational memory and hippocampal neurogenesis in mice. Hippocampus 2012;22:2095–100.
[36] Khan NA, Raine LB, Drollette ES, Scudder MR, Kramer AF, Hillman CH. Dietary fiber is positively associated with cognitive control among prepubertal children. World Rev Nutr Diet 2016;114:82–3.
[37] Van Der Werf YD, Tisserand DJ, Visser PJ, Hofman PAM, Vuurman E, Uylings HBM, et al. Thalamic volume predicts performance on tests of cognitive speed and decreases in healthy aging: a magnetic resonance imaging-based volumetric analysis. Cogn Brain Res 2001;11:377–85.